

Improving temperature-stable AZO–Ag–AZO multilayer transparent electrodes using thin Al layer modification

This article has been downloaded from IOPscience. Please scroll down to see the full text article.

2012 J. Phys. D: Appl. Phys. 45 505103

(<http://iopscience.iop.org/0022-3727/45/50/505103>)

View [the table of contents for this issue](#), or go to the [journal homepage](#) for more

Download details:

IP Address: 61.129.37.228

The article was downloaded on 21/11/2012 at 02:21

Please note that [terms and conditions apply](#).

Improving temperature-stable AZO–Ag–AZO multilayer transparent electrodes using thin Al layer modification

Lin Zhou, Xiaohong Chen, Feng Zhu, XinXing Sun and Zhuo Sun

Engineering Research Center for Nanophotonics and Advanced Instrument, Ministry of Education, and Department of Physics, East China Normal University, Shanghai 200062, People's Republic of China

E-mail: xhchen@phy.ecnu.edu.cn (X Chen)

Received 18 July 2012, in final form 25 September 2012

Published 19 November 2012

Online at stacks.iop.org/JPhysD/45/505103

Abstract

The thermal stability of AZO/Al/Ag/Al/AZO (5A) compared with AZO/Ag/AZO (3A) electrodes was significantly improved by introducing a thin Al layer at the interface between Ag and AZO layers. The rapidly deteriorated sheet resistance of 3A compared with 5A electrodes is roughly consistent with the XRD results of weaker intensity of the (1 1 1) Ag peak of 3A after annealing for 20 h at 300 or 500 °C for 10 min. The improved thermal stability of the 5A electrode is ascribed to the limitation function of Al atoms on Ag diffusion into the AZO layer. The polymer solar cells based on 5A compared with ITO electrodes showed a similar efficiency.

(Some figures may appear in colour only in the online journal)

1. Introduction

Flexible organic electronics, such as flexible organic light-emitting diodes and polymer solar cells (PSCs), have attracted considerable attention due to their light weight, low cost and their ability to flex, roll and fold for portability [1–3]. Transparent conducting oxide (TCO) electrodes, as key components in flexible organic electronics, should have mechanical robustness against substrate bending without resultant changes in its electrical and optical properties [4, 5]. The traditional TCO electrodes, such as tin-doped indium oxide (ITO), fluorine-doped tin oxide (FTO) and aluminium-doped zinc oxide (AZO), cannot completely meet flexible requirements because these electrodes are too brittle for their conductivity to quickly deteriorate after frequent flex [5]. To solve electrode brittleness, flexible dielectric/metal/dielectric (D/M/D) multilayer TCO electrodes [4–6], such as ITO/Ag/ITO, AZO/Ag/AZO, ZnO/Ag/ZnO and ITO/Au/ITO, have been suggested due to their very low resistivity and high transparency.

The D/M/D multilayer TCO electrodes can effectively suppress the reflection from the metal layer and gain high transmittance in the visible region due to the plasmon coupling between the metal layer and the dielectric layer. The

inserted metal layer sandwiched between dielectric layers would gradually evolve as a continuous, ultra-thin film from disconnected islands with increasing thickness [6, 7]. The quasi-continuous metal layer is important for metal-based TCO electrodes to quickly increase its conductivity and obtain low sheet resistance. By respectively optimizing the thickness of the metal and dielectric layers, metal-based TCO electrodes with high transmittance and low sheet resistance have been demonstrated [5–7]. Jeong and Kim reported that an indium-doped zinc oxide (IZO)/Ag/IZO multilayer electrode on a glass substrate can obtain $4.4 \Omega/\square$ and a maximum transmittance of 86% by optimizing Ag and IZO thickness [6]. Regioregular poly(3-hexylthiophene) (P3HT) and {6,6}-phenyl C₆₁-butyric acid methylester (PCBM) based bulk heterojunction PSCs fabricated from IZO/Ag/IZO electrodes showed a power conversion efficiency (PCE) of 3.25%, indicating that IZO/Ag/IZO electrode is a promising TCO electrode for optoelectronic devices and solar cells. In addition to low resistivity and high transmittance, temperature stability of TCO electrodes is also a critical requirement because electrodes should be able to withstand high temperatures under different environments, such as thermal annealing and long-term operation period of devices [8]. TCO electrodes based on some metal oxide combinations, such

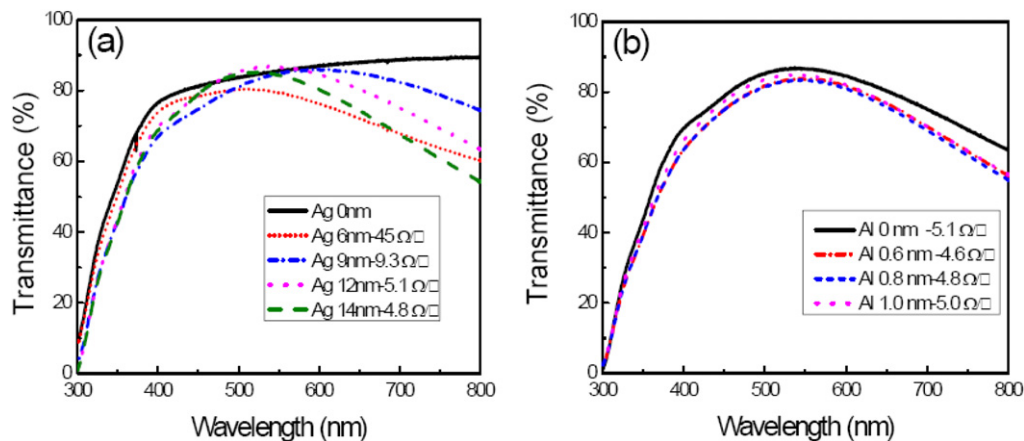


Figure 1. Optical transmittance and sheet resistance of 3A and 5A electrodes on the glass substrate. (a) 3A electrodes with different thicknesses of Ag layer, (b) 5A electrodes of 12 nm Ag layer with different thicknesses of modified Al layer.

as antimony-doped tin oxide (ATO)/AZO, FTO/ITO and ITO/ATO have been developed to improve thermal stability [9]. As for D/M/D multilayer electrodes, Dimopoulos *et al* reported that AZO/Au/AZO and AZO/Cu/AZO electrodes are more thermally stable than single AZO layer [8]. Sahu *et al* demonstrated that the deteriorated sheet resistance of Ag-based multilayer electrodes is attributed to diffusion of Ag atoms and oxidation of Ag layer [10]. However, there are few reports on how to limit metal atom diffusion and further improve the thermal stability of D/M/D multilayer TCO electrodes. In this paper, we developed an AZO/Al/Ag/Al/AZO (5A) electrode to improve the thermal stability. The thermal stability of AZO/Al/Ag/Al/AZO electrodes is significantly improved compared with that of AZO/Ag/AZO (3A) electrodes due to the limitation function of Al on Ag diffusion into the AZO layer.

2. Experimental

The 5A and 3A electrodes were respectively deposited on glass substrates by a magnetron sputtering system with a base pressure of 8×10^{-6} Torr. The thickness of two modified Al layers is always equal. The Ar flow rate and gas pressure were 15 sccm and 0.3 Pa during the sputtering process. The distance between the substrate and the target is 10 cm. AZO corresponds to a ZnO target doped with 2.0 wt% Al_2O_3 . The AZO layer was deposited by dc magnetron sputtering at the deposition rate of 2.95 \AA s^{-1} . The Ag and Al layers were deposited with deposition rates of 1 \AA s^{-1} and 0.2 \AA s^{-1} , respectively. The electrodes were annealed in a fibre resistance furnace (SX3-3-10) in ambient atmosphere.

The inverted PSC structure of electrode/ZnO/P3HT:PCBM/ MoO_3 /Al was fabricated to compare the effect of electrodes on the performance of PSCs. The active area of the device was 0.1 cm^2 . A 15 nm ZnO layer was deposited on top of the electrodes as an electron-transport/hole-blocking layer by RF magnetron sputtering at a deposition rate of 0.7 \AA s^{-1} . Solutions containing P3HT and PCBM with 1 : 0.8 weight ratio dissolved in 1,2-dichlorobenzene were spin-coated on top of the ZnO layer to form a 200 nm thick film and then kept in a

Petri dish for slow growth. After 12 h, the P3HT:PCBM films were annealed at 120°C for 10 min under ambient atmospheric conditions. 15 nm thick MoO_3 and 100 nm thick Al metallic layers were thermally deposited with a background pressure of 5×10^{-6} Torr.

Sheet resistance measurements were performed using the four-point probe technique and optical transmittance was measured using a UV-Vis-NIR spectrometer (UV3900, Unicam). A field emission scanning electron microscope (FESEM, S4300&EDX-350, Hitachi) was used to detect the surface morphology of the TCO electrodes at an operating voltage of 15 kV and cross-section at 3 kV. The crystal structures were studied using x-ray diffraction (XRD, Rigaku Ultima IV). Current-voltage characteristics were measured with a Newport solar simulator system under AM1.5G illumination of 100 mW cm^{-2} .

3. Results and discussion

The optical and resistance properties of the AZO/Ag/AZO electrodes are critically dependent on the thickness of the AZO and Ag layers, as well as sputtering conditions, such as the sputtering power, deposition rate and working pressure. Figure 1 shows the sheet resistance and optical transmittance of the 3A and 5A electrodes on glass substrates. The average sheet resistance of the electrodes decreases from 45 to 4.8Ω with increasing Ag thickness from 6 to 14 nm. The high sheet resistance of 3A at the Ag thickness of 6 nm is because the Ag layer exists in the form of isolated islands and randomly connected islands. The low transmittance at the Ag thickness of 6 nm is attributed to the absorption of the aggregated Ag islands [11]. The quasi-connected or connected Ag layer can result in high conductivity [4]. The optimized AZO(12 nm)/Ag(12 nm)/AZO(50 nm) electrode shows a reasonable low sheet resistance of $5.1 \Omega/\square$ and optical transmittance of 86% at the wavelength of 550 nm due to the surface plasmon resonance effect of the Ag layer [4, 7], as illustrated in figure 1(a). Figure 1(b) shows the optical transmittance and average sheet resistance of the 5A electrodes with increasing Al layer thickness at a constant Ag

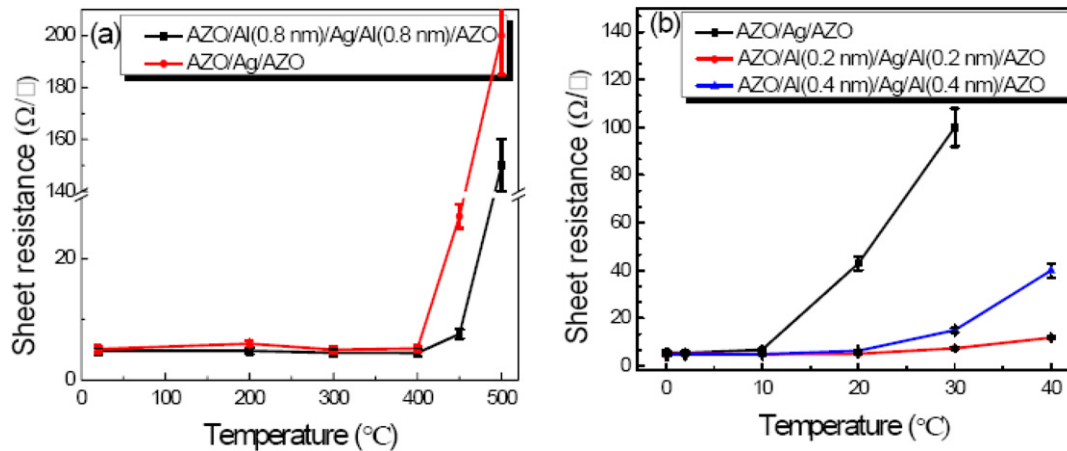


Figure 2. Averages and scatter for sheet resistance of 3A and 5A electrodes with 12 nm Ag layer under different annealing conditions: (a) different annealing temperatures for 10 min, (b) different annealing times at an annealing temperature of 300 $^{\circ}\text{C}$.

layer thickness of 12 nm. The transmittance of the optimized 5A electrodes is 85% at the wavelength of 550 nm, which approaches that of the optimized 3A electrode. The variation of the optical transmittance of the 5A electrodes with Al thickness from 0.2 to 1.0 nm is less than 3%, indicating that the inserted thin Al layer cannot significantly reduce its transmittance. The sheet resistance of 5A modified with a thin Al layer is very close to that of 3A with 12 nm Ag while considering their standard deviation.

Figure 2 shows the averages and scatter for sheet resistance of electrodes under different annealing conditions. The sheet resistance of 3A and 5A electrodes slightly dropped at an annealing temperature of 300 $^{\circ}\text{C}$ for 10 min and started increasing at 450 $^{\circ}\text{C}$, as shown in figure 2(a). The 5A electrode showed more thermal stability than the 3A electrode because the sheet resistance of 3A (27 Ω/\square) deteriorated more quickly than that of 5A (7.6 Ω/\square) at the annealing temperature of 450 $^{\circ}\text{C}$. However, the deteriorated sheet resistance of the 5A electrodes still occurred on annealing at 450 $^{\circ}\text{C}$. So the moderate annealing temperature of 300 $^{\circ}\text{C}$ was chosen to accurately check the thermal stability of 3A and 5A electrodes. The variance of sheet resistance of the 3A and 5A electrodes with different annealing times is shown in figure 2(b). The average sheet resistance of the 3A electrodes gradually increased from 10 h, and reached 43 Ω/\square after annealing for 20 h. But the sheet resistance of the 5A electrodes modified with Al layers from 0.2 to 0.8 nm remained almost constant within the annealing time of 20 h in the error range. This indicated that the 5A electrodes modified with an Al layer have better thermal stability than the 3A electrodes.

The sheet resistance of the 3A electrodes results from the resistance of the bottom AZO, Ag and top AZO layer coupled in parallel. The conduction characteristics of the AZO layer are primarily dominated by electrons generated by Al^{3+} ions on substitutional sites of Zn^{2+} ions and Al interstitial atoms as well as from oxygen vacancies and Zn interstitial atoms. As for 3A and 5A electrode systems, Ag could act as an acceptor and increase the electrical resistivity of the AZO electrode, if Ag^{+} ions diffuse into the AZO layer and substitute Zn^{2+} ions [12]. However, the Ag layer of 12 nm thickness

in situ is almost connected, as shown in figure 3. The sheet resistance of the 3A and 5A electrodes with a 12 nm Ag layer is primarily dominated by that of the Ag layer because the electrical resistivity of AZO ($5.7 \times 10^{-3} \Omega \text{ cm}$) is almost two orders of magnitude larger than that of the connected Ag layer ($3.7 \times 10^{-5} \Omega \text{ cm}$). Therefore, the increasing sheet resistance of the annealed 3A and 5A electrodes in figure 2 is primarily attributed to the deteriorated sheet resistance of the inserted Ag layer.

To investigate the fact that the 5A electrodes have better thermal stability than the 3A electrodes, we employed FESEM and XRD methods to analyse the 3A and 5A electrodes. Figure 3 shows the SEM images of Ag films at different annealing temperatures for 10 min. The Ag/AZO and Ag/Al/AZO films were deposited on silicon substrates, respectively. The morphology of the Ag layers is very similar to that of the Ag-modified Al layers at the same annealing temperature. The quasi-connected and connected Ag films without a capping AZO layer can easily aggregate above the annealing temperature of 300 $^{\circ}\text{C}$ for 10 min due to the surface melting effect [13]. The aggregated or isolated Ag islands can lead to a quick increase in its sheet resistance. This suggested that the Ag layer modified with Al compared with only the Ag layer does not have any advantage in inhibiting the aggregation of Ag films without a capping AZO layer.

The severely aggregating phenomenon of the Ag layer can be inhibited if a right capping layer is used, which can be supported by the cross-section FESEM images and XRD plots of the 3A and 5A films. Figure 4 shows the cross-section SEM images of 3A and 5A at different annealing temperatures for 10 min. The interfaces between the Ag and AZO layers cannot be clearly differentiated due to the low resolution of FESEM. The cross-section morphology of the 3A and 5A layers is roughly similar at room temperature (RT) and at the annealing temperature of 300 $^{\circ}\text{C}$. This means that the inserted Ag layer with the capping layer is still stable at 300 $^{\circ}\text{C}$. The morphology of 3A and 5A annealed at 450 $^{\circ}\text{C}$ becomes a little different and slightly rougher for 3A. The variable morphology is possibly ascribed to the diffusion of Ag atoms and/or aggregation of the Ag layer [10]. Unfortunately, the function of the inserted Al

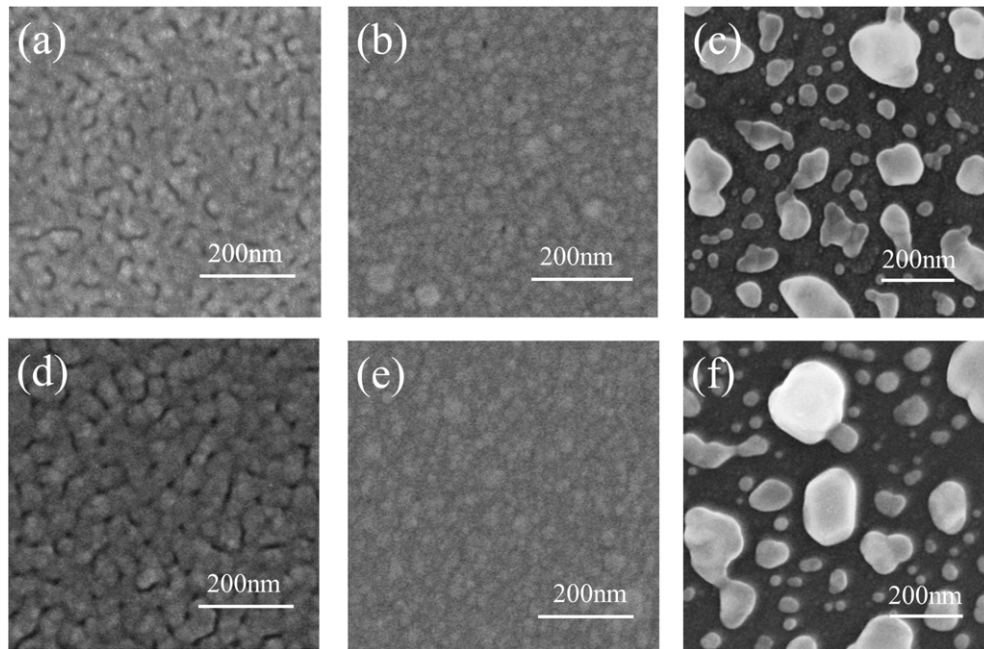


Figure 3. SEM images of Ag films at different annealing temperatures: Ag(12 nm)/AZO(12 nm) at (a) RT, (b) 200 °C, (c) 300 °C, and Ag(12 nm)/Al(0.6 nm)/AZO(12 nm) at (d) RT, (e) 200 °C and (f) 300 °C.

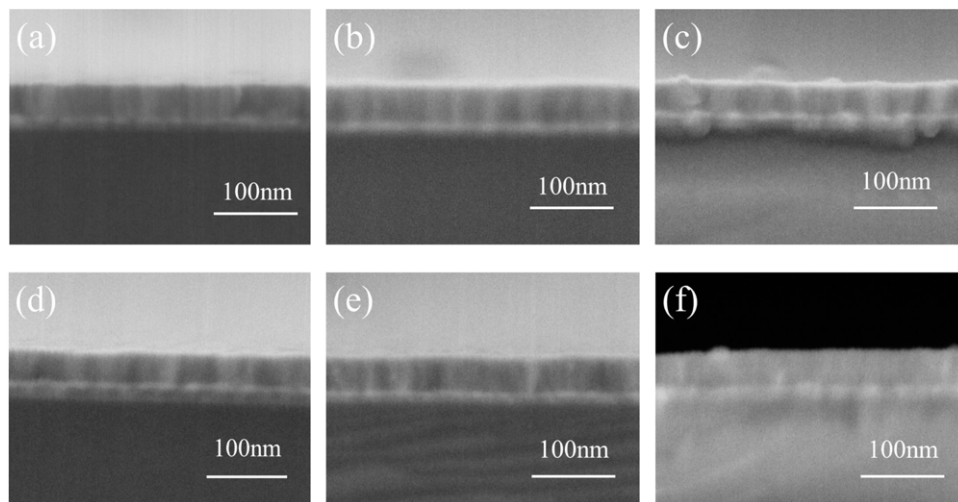


Figure 4. Cross-section SEM images of 3A at annealing temperatures of (a) RT, (b) 300 °C, (c) 450 °C, and 5A at (d) RT, (e) 300 °C, (f) 450 °C.

layer in limiting Ag diffusion and aggregation still cannot be clearly demonstrated due to blurred SEM images.

Figures 5(a) and (b) show the XRD plots of the 3A and 5A electrodes with increasing annealing temperature at a constant annealing time of 10 min. The (002) ZnO and (111) Ag peaks are observed for the samples. The (002) peaks of the 3A and 5A electrodes are expected to shift by $\sim 0.24^\circ$ to a larger 2θ value at room temperature compared with that of pure ZnO films and are further shifted with increasing annealing temperature. This is because some Zn^{2+} sites are substituted by Al^{3+} ions and more Zn^{2+} sites are substituted with increasing annealing temperature [14]. The intensity of the (002) ZnO and (111) Ag peaks increases remarkably and the full-width at half-maximum (FWHM) decreases slightly with increasing temperature from room temperature to 400 °C,

indicating better crystallinity and larger crystal sizes of AZO and Ag layers after annealing [7, 14]. The rapidly decreasing intensity of the (111) Ag peaks at 500 °C indicates that the Ag content decreases in the inserted Ag layer. The shortage of Ag content in the Ag layer can result in noncontinuous and isolated Ag islands, which are possibly responsible for the deteriorated sheet resistance of the 3A and 5A electrodes on annealing at 500 °C. The sharply narrower FWHM of the (111) Ag peak of the 5A electrode after annealing at 500 °C means that severely aggregated Ag islands exist. However, the deteriorated sheet resistance of 5A ($7.6 \Omega/\square$) and 3A ($27 \Omega/\square$) cannot be supported by XRD plots of annealing at 450 °C. Figures 5(c) and (d) show the XRD plots of the 3A and 5A electrodes with different annealing times at annealing temperature 300 °C. The intensity of the (111) Ag peak of

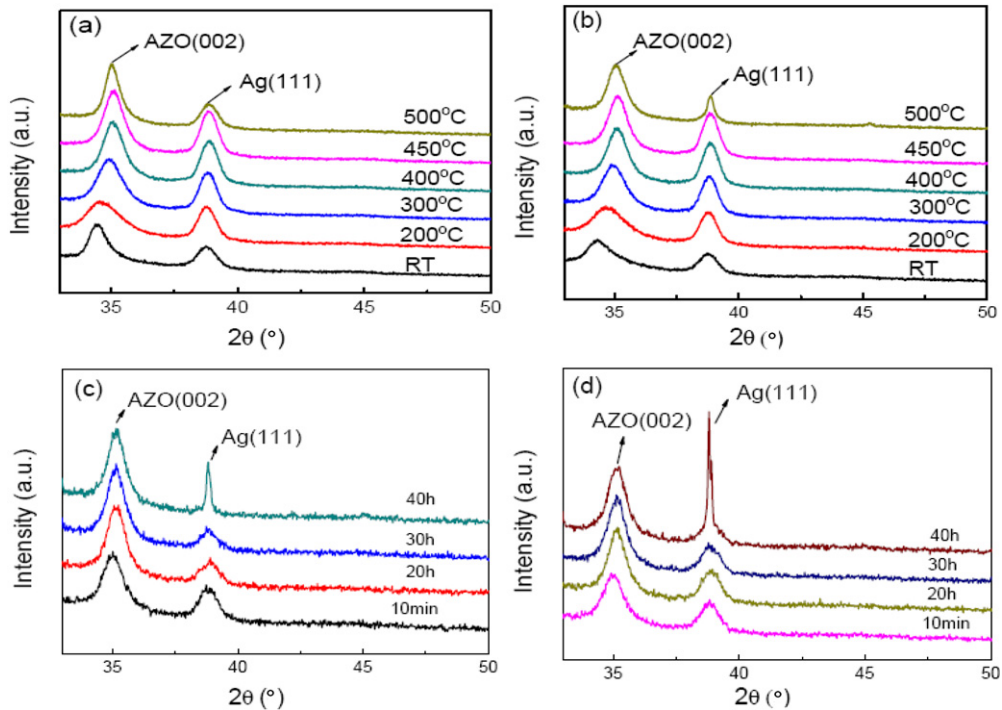


Figure 5. XRD plots of 3A and 5A electrodes with 12 nm Ag layer under different annealing conditions: (a) 3A and (b) 5A electrodes with different annealing temperatures for 10 min; (c) 3A and (d) 5A electrodes with different annealed times at 300 °C.

3A after annealing for 20 h compared with annealing for 10 min becomes significantly weaker, indicating that the Ag content decreases due to Ag diffusion. The intensity of the (1 1 1) Ag peak of the 5A electrodes remained constant after annealing for 20 h. Accordingly, the sheet resistance of 3A quickly increased from 5.3 to 43 Ω/\square , and that of the 5A electrodes remained almost constant after annealing for 20 h. The FWHM of the (1 1 1) Ag peaks of the 3A and 5A electrodes became significantly narrower after annealing for 40 h, which meant severe aggregation of Ag islands and resulted in quickly deteriorated sheet resistance of the 3A and 5A electrodes. The results suggested that the variance of intensity and FWHM of the (1 1 1) Ag peak is qualitatively consistent with the variance of sheet resistance of the 3A and 5A electrodes.

Generally, there are two possible paths to decrease the Ag content of the inserted Ag layer in 3A and 5A electrodes after annealing. One is the oxidation of Ag after annealing in ambient atmosphere. The peak of AgO_x cannot be observed in the XRD plots [15], indicating that oxidation of Ag is not the main path resulting in the deteriorated sheet resistance of 3A and 5A electrodes. The other is the diffusion of Ag atoms of the inserted Ag layer into the AZO layer [10]. Ag atoms can usually diffuse into the AZO layer as interstitial atoms during annealing, and even substitute Zn^{2+} ions at higher annealing temperatures. When an Al layer is inserted between the Ag and AZO layers, Al^{3+} atom can diffuse or substitute Zn^{2+} atoms more easily than Ag atoms because the ionic radius of Al^{3+} (53 pm) is far smaller than that of Ag^+ (126 pm) [15, 16]. This would possibly limit the diffusion of Ag atoms into the AZO layer during the annealing process, which makes 5A more thermally stable than the 3A electrodes.

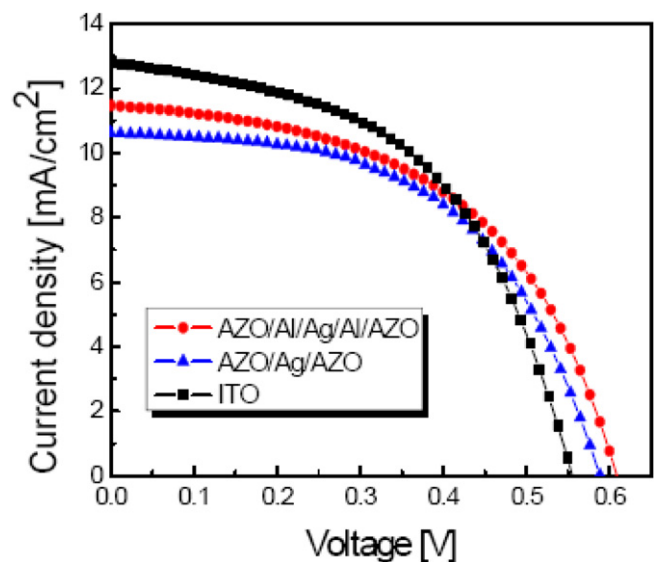


Figure 6. Current density–voltage curves of PSCs based on 5A, 3A and ITO electrodes.

To compare the effect of electrodes on the performance of PSCs, three kinds of inverted polymer solar cells based on 3A, 5A and ITO ($10 \Omega/\square$) electrodes were fabricated under the same preparation conditions. The inverted PSC structure is electrode/ZnO/P3HT : PCBM/MoO₃/Al. The current density–voltage (J – V) characteristics of the PSCs are shown in figure 6. The PCE values of the PSCs based on 5A, 3A and ITO are 3.54%, 3.36% and 3.63%, respectively. The averages and scatter for PSC parameters are listed in table 1. The PCE of the PSCs based on 5A is roughly comparable to that of the PSCs based on 3A and ITO. This suggested that the 5A

Table 1. Averages and scatter for parameters of PSCs based on ITO, 3A and 5A electrodes. Data in parentheses present the scatter absolute value of PSCs.

Test cell electrode	Efficiency (%)	J_{sc} (mA cm ⁻²)	V_{oc} (V)	Fill factor (%)
ITO	3.5 (0.3)	12.1 (0.7)	0.56 (0.02)	51 (2)
AZO/Al/Ag/Al/AZO	3.3 (0.3)	11.4 (0.7)	0.59 (0.02)	50 (2)
AZO/Ag/AZO	3.2 (0.2)	10.6 (0.5)	0.58 (0.03)	50 (3)

electrode modified with an Al layer has the same function as 3A and ITO electrodes, and can act as a promising alternative electrode in PSCs.

4. Conclusion

In summary, 3A and 5A TCO electrodes with low sheet resistance and high optical transmittance were fabricated by the magnetron sputtering method. The thermal stability of the 5A electrode modified with an Al layer is significantly improved compared with the 3A electrodes. The improved thermal stability of the 5A electrodes is primarily attributed to certain limitation on Ag diffusion into the AZO layer due to the inserted Al layer. The strategy of limiting Ag atom diffusion and/or Ag island aggregation is expected to improve the thermal stability of dielectric/metal/dielectric multilayer TCO electrodes and extend the operation time of PSCs resulting from deteriorated electrodes. The PCE of inverted PSCs based on 5A electrodes is comparable to that of ITO electrodes, indicating that the 5A electrode is a promising transparent conducting electrode for PSCs and optoelectronic devices.

Acknowledgments

This work was supported by the Natural Science Foundation of Shanghai Science and Technology Commission (grant No 11ZR1411300), Pujiang Talent Program of Shanghai Science and Technology Commission (grant No 11PJ1402700), Doctoral Fund of Ministry of Education of China (grant No 20110076120017) and SRF for ROCS, SEM.

References

- [1] Hübler A, Trnovec B, Zillger T, Ali M, Wetzold N, Mingebach M, Wagenpfahl A, Deibel C and Dyakonov V 2011 *Adv. Energy Mater.* **1** 1018–22
- [2] Chen X, Zhao C, Rothberg L and Ng M K 2008 *Appl. Phys. Lett.* **93** 123302
- [3] Espinosa N, Hösel M, Angmo D and Krebs F C 2012 *Energy Environ. Sci.* **5** 5117–32
- [4] Jeong J A, Park Y S and Kim H K 2010 *J. Appl. Phys.* **107** 023111
- [5] Choa S H, Cho C K, Hwang W J, Tae Eun K and Kim H K 2011 *Sol. Energy Mater. Sol. Cells* **95** 3442–9
- [6] Jeong J A and Kim H K 2009 *Sol. Energy Mater. Sol. Cells* **93** 1801–9
- [7] Park H K, Kang J W, Na S I, Kim D Y and Kim H K 2009 *Sol. Energy Mater. Sol. Cells* **93** 1994–2002
- [8] Dimopoulos T, Radnoczi G, Horváth Z and Brückl H 2012 *Thin Solid Films* **520** 5222–6
- [9] Montero J, Guillén C and Herrero J 2011 *Thin Solid Films* **519** 7564–7
- [10] Sahu D, Chen C, Lin S and Huang J L 2006 *Thin Solid Films* **515** 932–5
- [11] Zadsar M, Fallah H R, Mahmoodzadeh M H and Tabatabaei S V 2012 *J. Lumin.* **132** 992–7
- [12] Xue H, Xu X, Chen Y, Zhang G and Ma S 2008 *Appl. Surf. Sci.* **255** 1806–10
- [13] Sun X, Chen X, Zhang Z and Sun Z 2011 *Appl. Surf. Sci.* **258** 3785–8
- [14] Kim K H, Park K C and Ma D Y 1997 *J. Appl. Phys.* **81** 7764
- [15] Du Ahn B, Kang H S, Kim J H, Kim G H, Chang H W and Lee S Y 2006 *J. Appl. Phys.* **100** 093701
- [16] Park K C, Ma D Y and Kim K H 1997 *Thin Solid Films* **305** 201–9